

Theory of Optimal Learning Rate Schedules and Scaling Laws for a Random Feature Model

Blake Bordelon ^{* 1} Francesco Mori ^{* 1}

Abstract

Setting the learning rate for a deep learning model is a critical part of successful training, yet choosing this hyperparameter is often done empirically with trial and error. In this work, we explore a solvable model of optimal learning rate schedules for a powerlaw random feature model trained with stochastic gradient descent (SGD). We consider the optimal schedule $\eta_T^*(t)$ where t is the current iterate and T is the total training horizon. This schedule is computed both numerically and analytically (when possible) using optimal control methods. Our analysis reveals two regimes which we term the easy phase and hard phase. In the easy phase the optimal schedule is a polynomial decay $\eta_T^*(t) \simeq T^{-\xi}(1 - t/T)^\delta$ where ξ and δ depend on the properties of the features and task. In the hard phase, the optimal schedule resembles warmup-stable-decay with constant (in T) initial learning rate and annealing performed over a vanishing (in T) fraction of training steps. We investigate joint optimization of learning rate and batch size, identifying a degenerate optimality condition. Our model also predicts the compute-optimal scaling laws (where model size and training steps are chosen optimally) in both easy and hard regimes. Going beyond SGD, we consider optimal schedules for the momentum $\beta(t)$, where speedups in the hard phase are possible. We compare our optimal schedule to various benchmarks in our task including (1) optimal constant learning rates $\eta_T(t) \sim T^{-\xi}$ (2) optimal power laws $\eta_T(t) \sim T^{-\xi}t^{-\chi}$, finding that our schedule achieves better rates than either of these. Our theory suggests that learning rate transfer across training horizon depends on the structure of the model and task. We explore these ideas in simple experimental pretraining setups.

^{*}Equal contribution ¹Center of Mathematical Sciences and Applications, Harvard University, Cambridge, MA, USA. Correspondence to: Blake Bordelon <blake@cmsa.fas.harvard.edu>, Francesco Mori <francesco@cmsa.fas.harvard.edu>.

Preprint. February 5, 2026.

1. Introduction

Training deep learning models requires choosing many hyperparameters such as the learning rate, batch size, training horizon, total data, and architectural details, resulting in a complicated decision space. To make matters worse, it is challenging to characterize how these various hyperparameters jointly interact as one scales up the model size or training horizon. One strategy to reduce this complexity is to identify scaling protocols that allow for *transfer* of optimal hyperparameters, where small models can provide reliable proxies for tuning for large models. Such approximate hyperparameter transfer across model sizes can be achieved by principled parameterization and optimizer design (Yang et al., 2022; Bordelon et al., 2023; Yang et al., 2023; Dey et al., 2025). However, these schemes do not automatically lead to transfer over training horizons (Bjorck et al., 2024; Everett et al., 2024). In Figure 1 we illustrate the failure of transfer over training horizons T despite having successful transfer over model sizes (widths N). This failure motivates theory that can account for the behavior of optimal learning rates of SGD as the training horizon varies. Further, beyond optimal base learning rates themselves, one can also adopt a **learning rate schedule**. While many schedules such as linear decay, warmup-stable-decay, and cosine annealing are commonly used in practice, it is unclear under which conditions one should favor using a type of schedule over the other.

To address these questions in a theoretical framework, we make the following contributions:

- We analyze SGD dynamics in a powerlaw random feature model (Bordelon & Pehlevan, 2022; Bordelon et al., 2024; Paquette et al., 2024). We show that SGD fluctuations can lead to shifts in optimal learning rates across training horizons T that are **task and model dependent**.
- We characterize both numerically and analytically the **optimal learning rate annealing schedule** for SGD in our model using optimal control, minimizing the final test loss at step T . This analysis reveals two phases of tasks, easy and hard. For easy tasks, our schedule takes the form $\eta(t) = T^{-\xi}f(t/T)$, while for hard tasks our

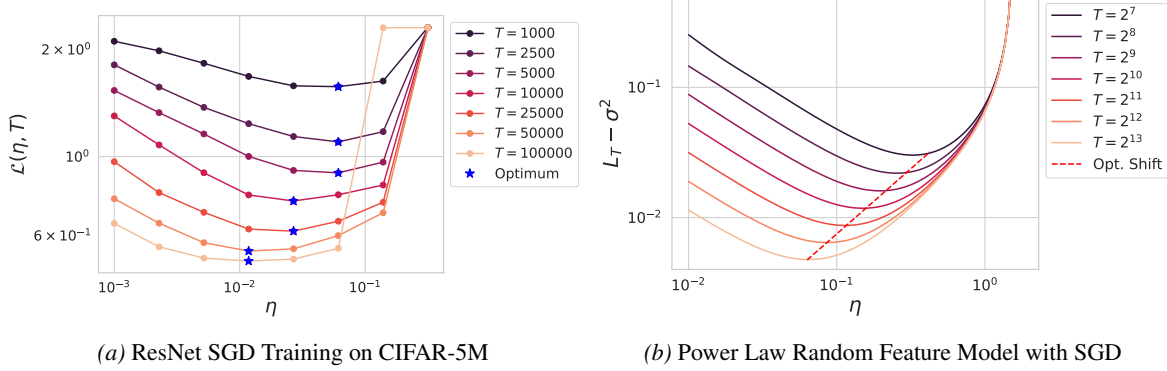


Figure 1. SGD learning rates do not automatically transfer over training horizons T . This motivates theory that can identify not only how to scale η with T , but also how to set the entire learning rate schedule $\eta(t)$ with T . (a) The loss of a deep ResNet trained on CIFAR-5M. (b) Test loss of a random feature model trained with SGD as a function of fixed learning rate η . The optimal learning rate shifts leftwards in this model, mimicking the behavior of the real network training (Bjorck et al., 2024).

schedule resembles warmup-stable-decay (WSD).

- We compare our optimal schedules to various benchmarks including optimized constant learning rate and optimal powerlaw schedules, finding that our schedules can achieve better scaling exponents.
- This analysis is generalized to optimal **batch size** schedules and optimal **momentum** schedules. Optimizing batch size and learning rate jointly enables a reduction in total wall-clock time, while optimizing the momentum parameter can provide an improvement in the scaling exponent for hard tasks beyond SGD.

1.1. Related Works

Based on the correspondence between neural networks in the lazy training regime (Chizat et al., 2019), many works have attempted to characterize neural scaling laws (Kaplan et al., 2020; Hoffmann et al.) by computing the generalization of random feature models with powerlaw features (Varre et al., 2021; Bordelon & Pehlevan, 2022; Bahri et al., 2024; Bordelon et al., 2024; Paquette et al., 2024; Lin et al., 2024; Ferbach et al., 2025). Several works have examined easy and hard phases of this model in the noise dominated regime (Dieuleveut & Bach, 2015; Lin & Rosasco, 2017). Notably, Pillaud-Vivien et al. (2018) demonstrated that optimal rates for SGD can be achieved in the hard phase with data repetition and model averaging strategies. Meterez et al. (2025) recently analyzed this model to motivate invariances between learning rate and batch sizes when designing schedules. (Qiu et al., 2025) identified a scaling collapse phenomenon where the compute optimal models exhibit universal loss dynamics across scales for a variety of learning rate schedules and developed a theoretical model of SGD that accounted for this supercollapse. Our work similarly utilizes this powerlaw random feature model, however we

study the *optimal learning rate schedule* for SGD using optimal control theory.

Optimal control theory provides a principled framework for deriving hyperparameter schedules in reduced theoretical models. Pioneering work in the 1990s characterized optimal learning rate schedules for two-layer neural networks within the teacher-student formalism (Saad & Rattray, 1997; Rattray & Saad, 1998). More recently, these techniques have been generalized to several hyperparameter protocols (Mori et al., 2025; Mignacco & Mori, 2025). Analogous optimization procedures have also recently been studied in deep linear networks (Carrasco-Davis et al., 2023) and cognitive science (Njaradi et al., 2026).

Most closely related to our work is (Li et al., 2025), which examined learning rate schedules within the context of power-law random feature models. However, their analysis was restricted to pre-defined, parametric schedules and did not address the theoretical derivation of the optimal control policy.

2. Setting

2.1. Power Law Linear Random Feature Model

We consider a random-feature model widely studied in the literature of scaling laws (Bordelon & Pehlevan, 2022; Bordelon et al., 2024; Lin et al., 2024; Paquette et al., 2024). Let the inputs $\mathbf{x} \in \mathbb{R}^D$ be drawn from a probability distribution $p(\mathbf{x})$. The associated labels are generated as

$$y(\mathbf{x}) = \mathbf{w}^* \cdot \psi(\mathbf{x}) + \sigma_0 z, \quad (1)$$

where $\sigma_0 > 0$ is the amplitude of the label noise and $z \sim \mathcal{N}(0, 1)$. The vector $\psi(\mathbf{x}) \in \mathbb{R}^M$ (with M possibly infinite) is a feature map and $\mathbf{w}^* \in \mathbb{R}^M$ a vector of parameters. We work in the feature eigenbasis, so that

$$\langle \psi_i(\mathbf{x}) \psi_j(\mathbf{x}) \rangle_{\mathbf{x} \sim p(\mathbf{x})} = \delta_{ij} \lambda_i. \quad (2)$$

We consider a linear student model $\hat{y}(\mathbf{x}) = \mathbf{w} \cdot \tilde{\psi}(\mathbf{x})$, with parameters $\mathbf{w} \in \mathbb{R}^N$ and projected features $\tilde{\psi}(\mathbf{x}) = \mathbf{G}\psi(\mathbf{x})$, where $\mathbf{G} \in \mathbb{R}^{N \times M}$ is a projection matrix. To describe model-size effects, we assume $N \leq M$ and that the top- N features are selected, i.e., $\mathbf{G} = [\mathbf{I}_N, \mathbf{0}_{N \times (M-N)}]$. We train via online stochastic gradient descent (SGD) on the square loss

$$\mathbf{w}_{t+1} = \mathbf{w}_t - \frac{\eta_t}{m_t} \sum_{\mu=1}^{m_t} \tilde{\psi}(\mathbf{x}_{\mu,t}) (\mathbf{w}_t \cdot \tilde{\psi}(\mathbf{x}_{t,\mu}) - y(\mathbf{x}_{t,\mu})), \quad (3)$$

with learning rate η_t and minibatch size m_t . The samples $\mathbf{x}_{\mu,t}$ and the label noise variables $z_{\mu,t}$ are assumed to be independent. The parameters are initialized to zero.

2.2. Analytical Expression for Test Loss Dynamics

Following (Bordelon & Pehlevan, 2022), for $k = 1 \dots N$, we define $c_{t,k} = \langle (w_{t,k} - w_k^*)^2 \rangle_{\mathcal{D}_{t-1}}$, where $\langle \cdot \rangle_{\mathcal{D}_{t-1}}$ indicates the average over all noise sources up to time $t-1$. Assuming that the features $\psi(\mathbf{x})$ are zero-mean Gaussian variables, one can show that the coefficients $c_{t,k}$ satisfy the recursion relation (Bordelon & Pehlevan, 2022)

$$\begin{aligned} c_{t+1,k} &= \left(1 - 2\eta_t \lambda_k + \eta_t^2 \frac{m_t + 1}{m_t} \lambda_k^2 \right) c_{t,k} \\ &+ \frac{\eta_t^2}{m_t} \lambda_k \sum_{\ell=1}^N \lambda_\ell c_{t,\ell} + \frac{\eta_t^2}{m_t} \sigma^2 \lambda_k, \end{aligned} \quad (4)$$

where we have defined the total irreducible noise as

$$\sigma^2 = \sigma_0^2 + \sum_{k=N+1}^M (w_k^*)^2 \lambda_k. \quad (5)$$

The test loss L_t at time t has the form

$$\begin{aligned} L_t &\equiv \langle \langle (\mathbf{w}^* \cdot \psi(\mathbf{x}) + \sigma_0 z - \mathbf{w} \cdot \tilde{\psi}(\mathbf{x}))^2 \rangle_{\mathcal{D}_{t-1}} \rangle_{\mathbf{x},z} \\ &= \sum_{k=1}^N c_{t,k} \lambda_k + \sigma^2. \end{aligned} \quad (6)$$

It is therefore sufficient to track $c_{t,k}$ in order to predict the test loss dynamics.

2.3. Power-law spectra

Motivated by empirical observations that natural data often exhibit power-law spectral decay (Bordelon & Pehlevan, 2022; Bahri et al., 2024), we assume power-law scalings for the data covariance eigenvalues and the teacher weights: $\lambda_k \sim k^{-b}$ and $(w_k^*)^2 \lambda_k \sim k^{-a}$, with exponents $a, b > 1$. These parameters characterize the effective dimension and difficulty of the learning task.

Under these assumptions, for a constant learning rate η and

batch size m , the excess loss scales as (see Appendix C):

$$L_T - \sigma^2 \sim (\eta T)^{-\frac{a-1}{b}} + \frac{\sigma^2 \eta}{m}, \quad (7)$$

where \sim denotes proportionality up to constant factors. Optimizing over a fixed learning rate yields the optimal constant strategy $\eta \sim T^{-(a-1)/(a+b-1)}$, which results in $L_T - \sigma^2 \sim T^{-(a-1)/(a+b-1)}$. A fundamental question is whether this scaling exponent can be improved by modulating the learning rate over time, and if so, what is the optimal schedule $\eta_T^*(t)$.

3. Optimal LR schedules via optimal control

We formulate the selection of the learning rate schedule as an optimal control problem aimed at minimizing the terminal generalization error L_T for a fixed training budget T . Initially, we focus on optimizing the learning rate $\eta_T(t)$ at a constant mini-batch size. Directly applying optimal control to the SGD dynamics in Eq. (3) is computationally intractable due to the high-dimensional and stochastic nature of the process. Instead, we optimize the control variable acting on the deterministic evolution of the variables $c_{t,k}$ derived in Eq. (4). For this analysis, we fix the model size to a large value ($N = 1000$ unless stated otherwise). The joint optimization of model size and training time (compute-optimal scaling) is discussed in Section 3.5.

3.1. Numerical optimal control

We first approach the problem numerically by optimizing the evolution equation (4) using a single-shooting method implemented in CasADi (Andersson et al., 2019), see Appendix F for details. This procedure allows us to identify the optimal learning rate schedules $\eta_T^*(t)$ for various training horizons T , as illustrated in Figures 2a and 2d. Crucially, we observe that across different regimes of data structure (parameterized by a and b), the optimal schedules achieve a higher scaling exponent compared to the optimal constant- η baseline.

3.2. Analytical derivation of optimal schedules

To determine the analytical form of the optimal schedule, we consider the continuous-time limit for large T (when taking this limit, we will often use the notation $\eta(t)$). Assuming that the learning rate decays sufficiently fast as $t \rightarrow T$ (see Appendix C), we can decompose the generalization error into bias and variance terms

$$L_T - \sigma^2 \sim \text{Bias}(T) + \text{Var}(T), \quad (8)$$

where

$$\text{Bias}(T) = \left(\int_0^T dt \eta(t) \right)^{-\frac{a-1}{b}}, \quad (9)$$

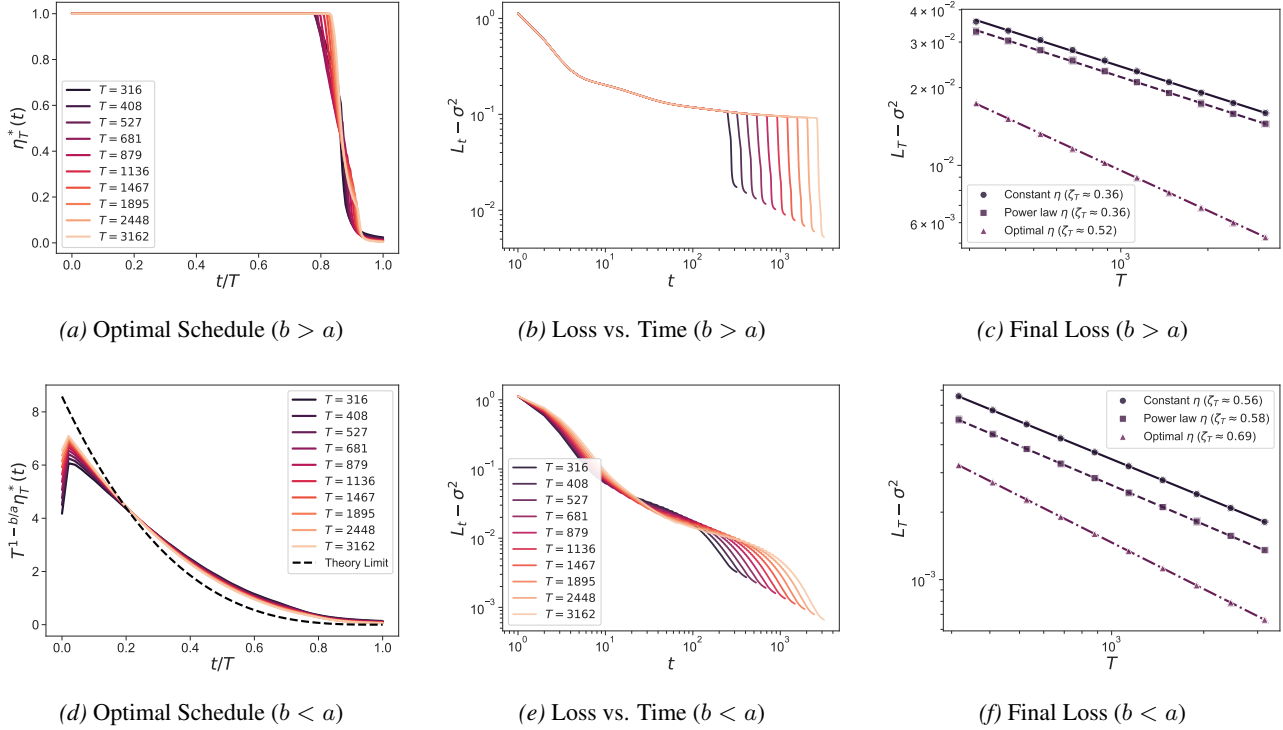


Figure 2. Comparison of optimal learning rate schedules in the hard (top row, $b > a$) and easy (bottom row, $b < a$) phases. **(a, d)** Profile of the optimal learning rate $\eta_T^*(t)$. In the hard phase **(a)**, the schedule maintains a constant maximum value for $t < t_s$ followed by a rapid annealing phase, where the annealing fraction $1 - t_s/T$ vanishes as $T \rightarrow \infty$ (see Fig. 7). In the easy phase **(d)**, the schedule collapses onto the scaling form $\eta_T^*(t) \approx T^{b/a-1} f(t/T)$ (dashed theoretical curve, see Eq. (12)). **(b, e)** Evolution of the loss over training time t for the optimal schedule. **(c, f)** Scaling of the final excess loss $L_T - \sigma^2$ with the training horizon T . The optimal schedule improves scaling exponent compared to the optimal constant and power-law baselines. Exponents obtained from numerical fit match theoretical predictions: for the constant and power-law case, $\zeta_T = \frac{a-1}{a+b-1}$ ($\zeta_T = 1/3$ for panel **(a)** and $\zeta_T = 5/9 \approx 0.56$ for panel **(d)**), for the optimal schedule $\zeta_T = \min(\frac{a-1}{a}, \frac{a-1}{b})$ ($\zeta_T = 0.5$ for panel **(a)** and $\zeta_T = 5/7 \approx 0.71$ for panel **(d)**). **Parameters:** $N = 1000$, $\eta_{\max} = 1$, $a = 3.5$, $m = 5$, with $b = 5$ (top row) and $b = 2$ (bottom row).

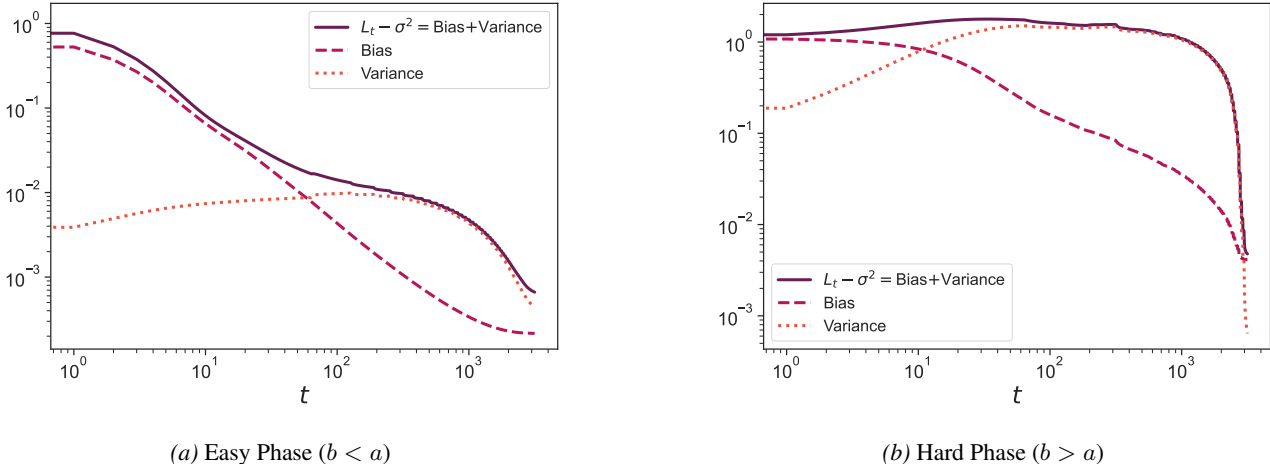


Figure 3. Decomposition of the excess loss $L_t - \sigma^2$ into bias and variance components. **(a)** In the easy phase ($b = 2, a = 3.5$), the optimal schedule minimizes bias and variance simultaneously throughout the training trajectory. **(b)** In the hard phase ($b = 5, a = 3.5$), the schedule minimizes the bias for the majority of the training time ($t < t_s$) where the learning rate is large, while the final annealing phase ($t > t_s$) is responsible for suppressing the variance. **Parameters:** $T = 3162$, $N = 1000$, $\sigma = 0.5$, $m = 5$.

and

$$\text{Var}(T) = \sigma^2 \int_0^T dt \frac{\eta^2(t)}{m(t)} \left(\int_t^T dt' \eta(t') \right)^{-\frac{2b-1}{b}}, \quad (10)$$

where $m(t)$ denotes the minibatch size at time t , that we take for now to be constant $m(t) = m$. To solve for the optimal schedule, we introduce the auxiliary state variable $\chi(t) = \int_t^T ds \eta(s)$, such that $\eta(t) = -\dot{\chi}(t)$ and $\chi(T) = 0$. The optimization problem can then be recast as minimizing the following functional of $\chi(t)$

$$L_T - \sigma^2 = \chi(0)^{-\frac{a-1}{b}} + \frac{\sigma^2}{m} \int_0^T dt \dot{\chi}^2(t) \chi(t)^{-\frac{2b-1}{b}}. \quad (11)$$

Since the Lagrangian density, i.e., the integrand in Eq. (11), explicitly depends on $\{\chi, \dot{\chi}\}$ but not on t , we can apply Noether's theorem (Gel'fand & Fomin, 2000) to identify a conserved quantity, which implies that the optimal trajectory satisfies the differential equation $\dot{\chi}(t) \propto \chi(t)^{(2b-1)/2b}$. The full analytical solution is detailed in Appendix B. To ensure the stability of the SGD dynamics, we additionally impose the hard constraint $\eta(t) \leq \eta_{\max}$. This constraint leads to two distinct scaling regimes depending on the parameters a and b . Following the terminology of (Pillaud-Vivien et al., 2018), we distinguish between an *easy phase* ($b < a$), where the constraint is asymptotically inactive, and a *hard phase* ($b > a$), where it plays a critical role.¹

Easy phase. In the regime where $b < a$, the optimal learning rate schedule admits the following scaling form in the large- T limit

$$\eta_T^*(t) = T^{b/a-1} f\left(\frac{t}{T}\right), \quad (12)$$

where the scaling function reads

$$f(z) = b \left[\frac{m}{b\sigma^2} \frac{\Gamma\left(\frac{a+b-1}{b}\right)}{\Gamma\left(2 - \frac{1}{b}\right)} \right]^{b/a} (1-z)^{2b-1}, \quad (13)$$

and $\Gamma(\cdot)$ is the gamma function. This solution corresponds to a schedule that decays as a polynomial of the time-to-go $T - t$. This type of schedule is commonly known as *polynomial decay* and has been used in a variety of applications (Wu & Liu, 2023).

As illustrated in Fig. 2d, our numerical optimization results converge to this analytical prediction as T increases. For this optimal schedule, the generalization error scales as $L_T - \sigma^2 \sim T^{-(a-1)/a}$, improving the scaling exponent compared to the optimal constant- η benchmark.

¹We note that this easy/hard distinction is focused on the behavior of label noise SGD and differs from other notions of easy and hard phases such as diverging RKHS norm (Paquette et al., 2024; Bordelon et al., 2025).

Hard phase. For $b > a$, the unconstrained optimum diverges, forcing the stability constraint $\eta(t) \leq \eta_{\max}$ to become active. The optimal schedule is

$$\eta_T^*(t) = \begin{cases} \eta_{\max} & t < t_s, \\ \eta_{\max} \left(\frac{1-t/T}{1-t_s/T} \right)^{2b-1} & t > t_s, \end{cases} \quad (14)$$

where the annealing phase duration scales as $1 - t_s/T \sim T^{-\frac{b-a}{2b-1}}$, in agreement with the schedules derived numerically (see Fig. 7). Interestingly, this protocol closely resembles a *warmup-stable-decay* (WSD) schedule (Hu et al., 2024) and yields a generalization error $L_T - \sigma^2 \sim T^{-(a-1)/b}$, outperforming the optimal constant- η baseline.

Depending on the spectral properties of the data, the optimal learning rate schedule adopts either a polynomial decay or a WSD profile. To understand these distinct behaviors, it is instructive to analyze the bias-variance decomposition shown in Fig. 3. The optimal schedule balances the reduction of bias, which benefits from larger learning rates (see Eq. (9)), against the variance, which requires annealing as $t \rightarrow T$ (see Eq. (10)). This trade-off requires the late-stage annealing observed in both schedules.

In the hard phase ($b > a$), the slow decay of the bias implies that the unconstrained optimal learning rate would grow as $T^{b/a-1}$ for large T . This divergence activates the stability constraint $\eta_T(t) \leq \eta_{\max}$, resulting in the WSD profile. While the easy phase schedule gradually decays to minimize both error components simultaneously, the hard phase strategy dedicates the majority of the training budget to maximizing bias suppression via a constant, maximal learning rate, compressing the variance-reducing annealing into a vanishing fraction of the total training time. In both regimes, a critical implication is that the optimal schedule relies on a fixed training horizon T . Anytime protocols, which are agnostic to the total budget, cannot effectively postpone variance minimization. The advantage of horizon-dependent schedules has been previously observed in convex optimization (Jain et al., 2019; Defazio et al., 2023).

Previous works have rationalized the effectiveness of the WSD schedule by conjecturing a “river valley” loss landscape (Wen et al., 2024; Liu et al., 2025). Here, we demonstrate that WSD is the optimal strategy in the hard phase, providing an alternative explanation for its effectiveness based on balancing demands of bias and variance reduction.

3.3. Comparison with benchmarks

Having established that the optimal schedule improves the scaling exponent relative to any constant learning rate strategy, we extend our comparison to a broader class of protocols. In Appendix C, we analyze power-law schedules of the form $\eta_T(t) \sim T^{-\xi} t^{-\delta}$, optimizing the exponents ξ and δ to

Phase	Constant LR	Powerlaw	Optimal
Easy ($a > b$)	$\frac{a-1}{a-1+b}$	$\frac{a-1}{a-1+b}$	$\frac{a-1}{a}$
Hard ($a < b$)	$\frac{a-1}{a-1+b}$	$\frac{a-1}{a-1+b}$	$\frac{a-1}{b}$

Table 1. Comparison of scaling exponents ζ_T for the loss as a function of training horizon $L_T - \sigma^2 \sim T^{-\zeta_T}$ for different types of schedules. Constant LR refers to $\eta_T(t) \sim T^{-\xi}$ and powerlaw refers to $\eta_T(t) \sim T^{-\xi}t^{-\delta}$, where the exponents ξ and δ are chosen optimally in each case, and optimal is the schedule we derive from optimal control.

minimize the final loss. We demonstrate that even the best-performing power-law schedule asymptotically recovers the same scaling behavior as the optimal constant- η strategy. Consequently, our derived optimal schedule strictly outperforms the entire family of power-law benchmarks (see Table 1). Our schedules saturate information theoretically optimal rates in the easy phase, but not the hard phase where $b > a$ (Fischer & Steinwart, 2020). Pillaud-Vivien et al. (2018) show a combination of data repetition and model averaging can improve the rates in the hard phase to saturate the theoretically optimal rate.

Generalizing beyond the specific optimal schedule derived in Eq. (12), we investigate the sensitivity of the performance to the choice of the profile function within the general scaling $\eta_T(t) = T^{-\xi}g(t/T)$. In Appendix C, we show that the specific shape of $g(z)$ does not change the scaling exponent, provided it decays faster than $(1-z)^{b-1}$ as $z \rightarrow 1$. The prefactor exponent ξ must be chosen as $\xi = \max[0, 1-b/a]$ (using a different value would result in suboptimal scaling). Under these conditions, the generic schedule recovers the optimal scaling exponents in both the easy and hard regimes, differing from the optimal error only by a constant prefactor.

3.4. Joint optimization of learning rate and batch size

Our analysis extends naturally to the joint optimization of the learning rate $\eta(t)$ and minibatch size $m(t)$ under a fixed data budget $B_{\text{tot}} = \int_0^T dt m(t)$. In this setting, the wall-clock time T is treated as a free variable. As detailed in Appendix D, the optimization yields a degenerate family of solutions satisfying the relation $m(t) \propto \eta(t)\chi(t)^{-1+1/(2b)}$. This manifold of solutions includes the fixed-batch strategy derived previously. However, following (Meterez et al., 2025), we can break this degeneracy by selecting the specific schedule that minimizes the wall-clock time T required to achieve the optimal performance. This criterion implies fixing the learning rate at its maximum stable value, $\eta(t) = \eta_{\max}$, which dictates the following batch-size schedule:

$$m_T^*(t) = \frac{B_{\text{tot}}}{2bT} \left(1 - \frac{t}{T}\right)^{\frac{1}{2b}-1}, \quad (15)$$

corresponding to an increasing batch size during training. This type of procedure, known as a *batch ramp*, has been

empirically proposed (Smith et al., 2017) but is derived here by a principled method.

The wall-clock time should be chosen to scale with the data budget as $T \sim B_{\text{tot}}^{b/a}$ for $b < a$ and $T \sim B_{\text{tot}}$ for $b > a$. Crucially, while the joint optimization reduces wall-clock time, it preserves the fundamental scaling of the generalization error with respect to the sample budget B_{tot} . Specifically, we recover $L_T - \sigma^2 \sim B_{\text{tot}}^{-(a-1)/a}$ in the easy phase ($b < a$) and $L_T - \sigma^2 \sim B_{\text{tot}}^{-(a-1)/b}$ in the hard phase ($b > a$), matching the scaling laws obtained by optimizing η at fixed m . However, a significant distinction emerges when analyzing the scaling with respect to wall-clock time. In the hard phase, the error scaling with T remains unchanged relative to the fixed-batch optimal strategy ($L_T - \sigma^2 \sim T^{-(a-1)/b}$). In contrast, in the easy phase, the joint optimization yields a strictly improved scaling of $L_T - \sigma^2 \sim T^{-(a-1)/b}$ (compared to $L_T - \sigma^2 \sim T^{-(a-1)/a}$).

3.5. Compute-optimal scaling

We next address the problem of jointly scaling the model size N and the data budget B_{tot} to minimize the generalization error L_C under a fixed compute budget $C = B_{\text{tot}}N$. Using Eq. (5), for $M \gg N \gg 1$, the effective noise variance scales as $\sigma^2 \sim \sigma_0^2 + N^{1-a}$. Consequently, in the easy phase, the excess loss scales as $L_T - \sigma_0^2 \sim B_{\text{tot}}^{-(a-1)/a} + N^{1-a}$. Balancing these terms yields the compute-optimal allocation $B_{\text{tot}} \sim C^{a/(a+1)}$ and $N \sim C^{1/(a+1)}$. This results in an optimal error scaling of $L_C - \sigma_0^2 \sim C^{-(a-1)/(a+1)}$. Similarly, in the hard phase, the loss scales as $L_T - \sigma_0^2 \sim B_{\text{tot}}^{-(a-1)/b} + N^{1-a}$. Optimizing this tradeoff leads to $B_{\text{tot}} \sim C^{b/(b+1)}$ and $N \sim C^{1/(b+1)}$, yielding a final error scaling of $L_C - \sigma_0^2 \sim C^{-(a-1)/(b+1)}$. These theoretical scaling laws are verified in Fig. 4.

3.6. Optimal Momentum Schedules Compared to SGD

We also study momentum with time varying learning rates η_t and momentum β_t which generate the update equations for parameters \mathbf{w}_t

$$\begin{aligned} \mathbf{w}_{t+1} &= \mathbf{w}_t + \eta_t \mathbf{v}_t \\ \mathbf{v}_t &= (1 - \beta_t) \mathbf{v}_{t-1} + \beta_t \mathbf{g}_t \\ \mathbf{g}_t &\equiv \frac{1}{m_t} \sum_{\mu=1}^{m_t} \tilde{\psi}(\mathbf{x}_{t,\mu}) \left(y(\mathbf{x}_{t,\mu}) - \mathbf{w}_t \cdot \tilde{\psi}(\mathbf{x}_{t,\mu}) \right) \end{aligned} \quad (16)$$

We optimize the loss at timestep T over the choices of $\{(\eta_t, \beta_t)\}_{t=1}^T$. Using similar methods to the analysis we used for SGD, we can compute the test loss by tracking three correlation variables $\{C_{k,t}, R_{k,t}, V_{k,t}\}$ for each eigendirec-

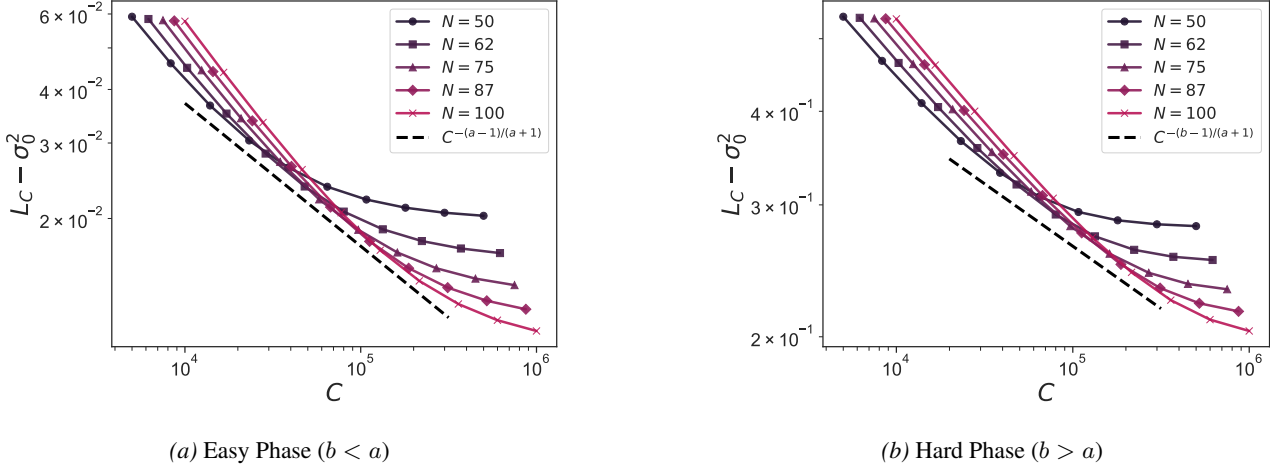


Figure 4. Compute optimal scaling. Residual loss $L_C - \sigma_0^2$ as a function of the compute $C = NT$ for different values of the model size N . The dashed lines indicate the theoretical prediction. **Parameters:** $\sigma = 0.5$, $m = 5$. In the easy phase $b = 1.5$ and $a = 2$, in the hard phase $b = 2$ and $a = 1.5$.

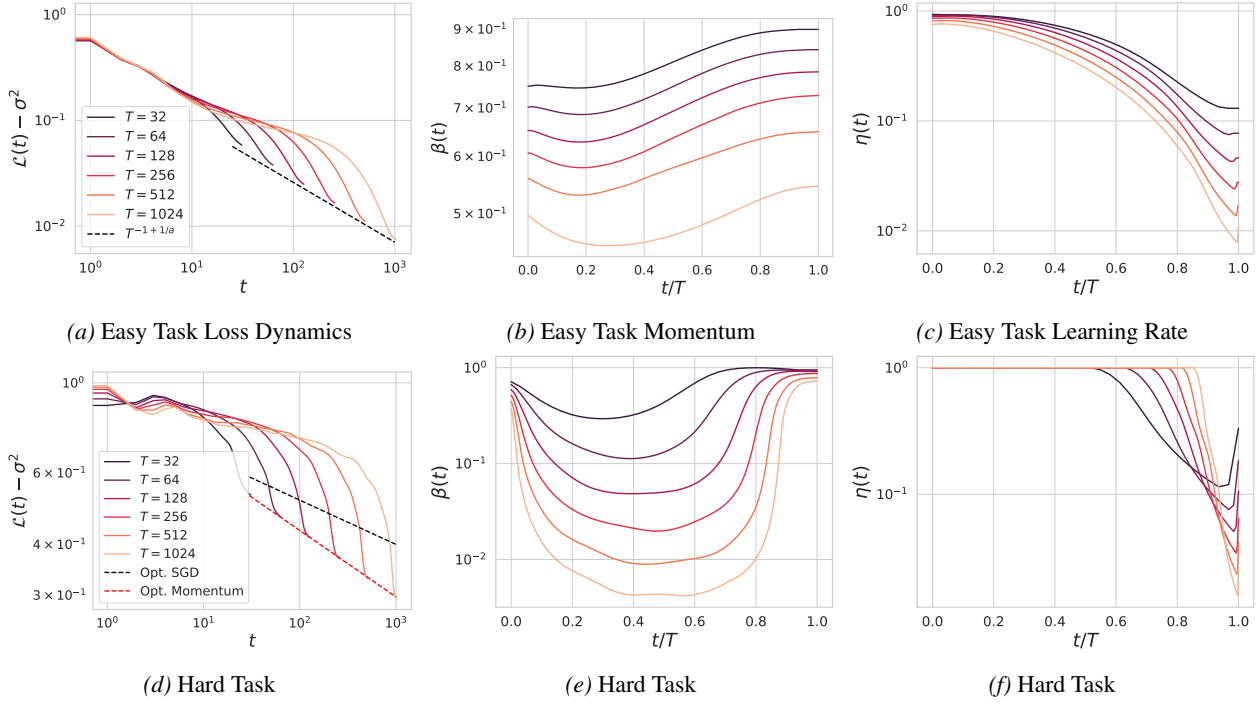


Figure 5. Optimal Schedule and loss dynamics for SGD + momentum. (a) For the easy task regime, the numerically optimized schedule achieves the same scaling law as SGD with optimal schedule $L_T - \sigma^2 \sim T^{-1+1/a}$. (b) The optimal momentum dynamics vary significantly across T but only weakly vary with t . (c) The learning rate for optimal momentum schedules anneals similarly to SGD in the easy phase. (d) In the hard phase, the scaling law for the loss obtained by jointly optimizing momentum and learning rate is better than the SGD rate $T^{-(a-1)/b}$. (e)-(f) Near the end of training, the momentum variable increases and the learning rate rapidly decreases.

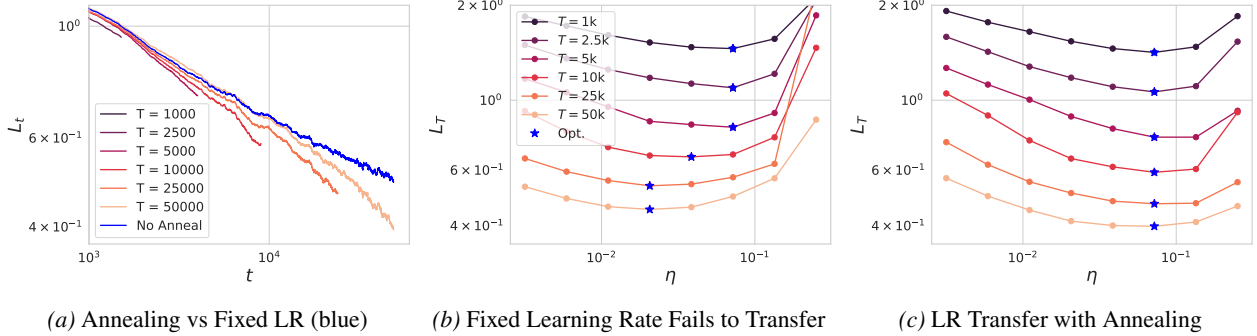


Figure 6. We plot width $N = 32$ depth 12 convolutional ResNets trained with SGD with batch size $m = 32$. (a) Cross-entropy loss dynamics as a function of training time t for fixed learning rate (blue) and polynomial annealing schedule set to training horizon T . The final loss follows a better trend when using the annealing schedule. (b) Loss as a function of (η, T) and for fixed learning rate. The optimal learning rate decreases with T . (c) For polynomial annealing schedules, the optimal base learning rate is approximately constant across horizons T , consistent with our model in the hard phase. Further, the best performance achieved at T iterations is noticeably improved compared to constant learning rate.

tion k . These variables are defined as

$$\begin{aligned} C_{k,t} &= \langle (w_{k,t} - w_k^*)^2 \rangle \\ R_{k,t} &= \langle v_{k,t} (w_k^* - w_{k,t}) \rangle \\ V_{k,t} &= \langle (v_{k,t})^2 \rangle \end{aligned} \quad (17)$$

which collectively evolve as a linear dynamical system that depends on $\lambda_k, w_k^*, \eta_t, \beta_t$ and m . From this dynamical system, we can obtain the loss dynamics $L_T - \sigma^2 = \sum_k \lambda_k C_{k,T}$, enabling use of optimal control. Recent work has demonstrated that allowing β to depend on time can improve scaling laws in this powerlaw random feature model (Ferbach et al., 2025). Instead of a preset schedule for β_t , we investigate the *optimal control* policy for η_t and β_t . We plot the result for easy and hard tasks in Figure 5, finding it differs from the anytime powerlaw schedule used by (Ferbach et al., 2025). We find that the optimal control learning rate for easy tasks exhibits phenomenology remarkably similar to optimal SGD. However, for hard tasks, we find that optimizing the momentum schedule β_t in addition to the learning rate schedule η_t provides an improvement to the scaling law with T . The optimal momentum variables β_t in either case show an initial transient decrease before a final increase as $t/T \rightarrow 1$.

4. Experiments in Deep Networks

We study a simple setup of CIFAR-5M (an extended version of CIFAR-10 that allows one-pass training) image classification in a deep convolutional ResNet (Nakkiran et al., 2020). We train with SGD using either fixed learning rate or a polynomial decay schedule, consistent with our optimal schedule. In Figure 6, we plot a comparison of the learning rate transfer for fixed learning rate schedules compared to polynomial decay. In Figure 6 (a) we show that the loss dynamics L_t for fixed learning rate (blue) can be outper-

formed at the same base learning rate by annealing with a schedule that decays to zero as $t/T \rightarrow 1$. In Figure 6 (b), we plot the optimal learning rate as a function of T for constant learning rate, which shifts left. Lastly, when using an annealing schedule we find that the optimal learning rate is approximately constant and the best performance at each value of T is improved compared to fixed learning rate. These observations are consistent with the behavior of our theoretical model in the hard phase since the optimal base learning rate is approximately constant. Based on the spectral analysis of the NTK for ResNets on CIFAR-5M from (Bordelon et al., 2024), it is reasonable to expect this problem-architecture pair to fall in the hard phase. We note that our theory *does not generally predict transfer of base learning rates*, since in the easy phase, the optimal base learning rate will still scale as a powerlaw in T .

5. Conclusions

We theoretically analyzed the optimal learning rate schedule for a simple random feature model. Our results utilized optimal control methods, which enabled optimization over the full trajectory of the learning dynamics. This model recapitulated schedules often observed in practice including polynomial decay schedules and warmup-stable-decay. Further, we explored optimal batch size and optimal momentum schedules, finding possible improvements in wall-clock time or training horizon scaling laws respectively.

Limitations and Future Directions While our analysis provided some insights into the behavior of SGD under different annealing schedules and different phases of task difficulty, there are several limitations to the present work. First, our current theory is focused on describing linear models trained with SGD. This can only capture optimization behaviors of neural networks operating in the lazy/kernel regime and also fails to capture the behavior of more sophis-

ticated optimizers such as Adam or preconditioned optimizers like Muon, Shampoo, or SOAP (Kingma & Ba, 2014; Jordan et al., 2024; Gupta et al., 2018; Vyas et al., 2024). Second, while our numerical solution to optimal momentum revealed an improvement in the scaling law exponent, we have not yet identified analytically what this improved exponent is for the hard phase. Lastly, we provided experiments of ResNets on CIFAR-5M that resemble our toy model in the hard phase. It would be interesting to identify naturalistic tasks (commonly studied architecture/optimizer/dataset pairs) that resemble the easy phase where both annealing and scaling the base learning rate are necessary to achieve optimal scaling laws.

Software and Data

We utilized the CasADi software package for numerical constrained optimal control problems (Andersson et al., 2019), for details see Appendix F. The implementation is available in the supplementary material. We used the CIFAR-5M dataset for our ResNet experiments (Nakkiran et al., 2020). Code to reproduce the experiments can be found at <https://github.com/blakebordelon/opt-control-sgd-rf>.

Acknowledgements

The authors thank Alex Atanasov, Francesca Mignacco, and Clarissa Lauditi for useful feedback on the manuscript. This work was supported by the Center of Mathematical Sciences and Applications (CMSA) at Harvard University.

Impact Statement

This paper presents work whose goal is to advance the field of Machine Learning. There are many potential societal consequences of our work, none of which we feel must be specifically highlighted here.

References

- Andersson, J. A., Gillis, J., Horn, G., Rawlings, J. B., and Diehl, M. Casadi: a software framework for nonlinear optimization and optimal control. *Mathematical Programming Computation*, 11(1):1–36, 2019.
- Bahri, Y., Dyer, E., Kaplan, J., Lee, J., and Sharma, U. Explaining neural scaling laws. *Proceedings of the National Academy of Sciences*, 121(27):e2311878121, 2024.
- Bjorck, J., Benhaim, A., Chaudhary, V., Wei, F., and Song, X. Scaling optimal lr across token horizons. *arXiv preprint arXiv:2409.19913*, 2024.
- Bordelon, B. and Pehlevan, C. Learning curves for SGD on structured features. In *International Conference on Learning Representations*, 2022. URL <https://openreview.net/forum?id=WPI2vbkA13Q>.
- Bordelon, B., Noci, L., Li, M. B., Hanin, B., and Pehlevan, C. Depthwise hyperparameter transfer in residual networks: Dynamics and scaling limit. *arXiv preprint arXiv:2309.16620*, 2023.
- Bordelon, B., Atanasov, A., and Pehlevan, C. A dynamical model of neural scaling laws. In *Forty-first International Conference on Machine Learning*, 2024. URL <https://openreview.net/forum?id=nb0Y10mtRc>.
- Bordelon, B., Atanasov, A., and Pehlevan, C. How feature learning can improve neural scaling laws. *Journal of Statistical Mechanics: Theory and Experiment*, 2025(8):084002, 2025.
- Carrasco-Davis, R., Masís, J., and Saxe, A. M. Meta-learning strategies through value maximization in neural networks. *arXiv preprint arXiv:2310.19919*, 2023.
- Chizat, L., Oyallon, E., and Bach, F. On lazy training in differentiable programming. *Advances in neural information processing systems*, 32, 2019.
- Defazio, A., Cutkosky, A., Mehta, H., and Mishchenko, K. Optimal linear decay learning rate schedules and further refinements. *arXiv preprint arXiv:2310.07831*, 2023.
- Dey, N., Zhang, B. C., Noci, L., Li, M., Bordelon, B., Bergsma, S., Pehlevan, C., Hanin, B., and Hestness, J. Don’t be lazy: Completep enables compute-efficient deep transformers. *arXiv preprint arXiv:2505.01618*, 2025.
- Dieuleveut, A. and Bach, F. Non-parametric stochastic approximation with large step sizes. *Annals of Statistics*, 44(4), 2015.
- Everett, K., Xiao, L., Wortsman, M., Alemi, A. A., Novak, R., Liu, P. J., Gur, I., Sohl-Dickstein, J., Kaelbling, L. P., Lee, J., et al. Scaling exponents across parameterizations and optimizers. *arXiv preprint arXiv:2407.05872*, 2024.
- Ferbach, D., Everett, K., Gidel, G., Paquette, E., and Paquette, C. Dimension-adapted momentum outscals sgd. *arXiv preprint arXiv:2505.16098*, 2025.
- Fischer, S. and Steinwart, I. Sobolev norm learning rates for regularized least-squares algorithms. *Journal of Machine Learning Research*, 21(205):1–38, 2020.
- Gel’fand, I. M. and Fomin, S. V. *Calculus of Variations*. Dover Publications, 2000.
- Gupta, V., Koren, T., and Singer, Y. Shampoo: Preconditioned stochastic tensor optimization. In *International Conference on Machine Learning*, pp. 1842–1850. PMLR, 2018.

- Hoffmann, J., Borgeaud, S., Mensch, A., Buchatskaya, E., Cai, T., Rutherford, E., de Las Casas, D., Hendricks, L. A., Welbl, J., Clark, A., et al. Training compute-optimal large language models.
- Hu, S., Tu, Y., Han, X., He, C., Cui, G., Long, X., Zheng, Z., Fang, Y., Huang, Y., Zhao, W., et al. Minicpm: Unveiling the potential of small language models with scalable training strategies. *arXiv preprint arXiv:2404.06395*, 2024.
- Jain, P., Nagaraj, D., and Netrapalli, P. Making the last iterate of sgd information theoretically optimal. In *Conference on Learning Theory*, pp. 1752–1755. PMLR, 2019.
- Jordan, K., Jin, Y., Boza, V., You, J., Cesista, F., Newhouse, L., and Bernstein, J. Muon: An optimizer for hidden layers in neural networks, 2024. URL <https://kellerjordan.github.io/posts/muon/>.
- Kaplan, J., McCandlish, S., Henighan, T., Brown, T. B., Chess, B., Child, R., Gray, S., Radford, A., Wu, J., and Amodei, D. Scaling laws for neural language models. *arXiv preprint arXiv:2001.08361*, 2020.
- Kingma, D. P. and Ba, J. Adam: A method for stochastic optimization. *arXiv preprint arXiv:1412.6980*, 22, 2014.
- Li, B., Chen, F., Huang, Z., Wang, L., and Wu, L. Unveiling the role of learning rate schedules via functional scaling laws. *arXiv e-prints*, pp. arXiv–2509, 2025.
- Lin, J. and Rosasco, L. Optimal rates for multi-pass stochastic gradient methods. *Journal of Machine Learning Research*, 18(97):1–47, 2017.
- Lin, L., Wu, J., Kakade, S. M., Bartlett, P., and Lee, J. D. Scaling laws in linear regression: Compute, parameters, and data. In *The Thirty-eighth Annual Conference on Neural Information Processing Systems*, 2024. URL <https://openreview.net/forum?id=PH7sdEanXP>.
- Liu, Z., Liu, Y., Gore, J., and Tegmark, M. Neural thermodynamic laws for large language model training. *arXiv preprint arXiv:2505.10559*, 2025.
- Meterez, A., Morwani, D., Wu, J., Oncescu, C.-A., Pehlevan, C., and Kakade, S. Seesaw: Accelerating training by balancing learning rate and batch size scheduling. *arXiv preprint arXiv:2510.14717*, 2025.
- Mignacco, F. and Mori, F. A statistical physics framework for optimal learning. *arXiv preprint arXiv:2507.07907*, 2025.
- Mori, F., Mannelli, S. S., and Mignacco, F. Optimal protocols for continual learning via statistical physics and control theory. *Journal of Statistical Mechanics: Theory and Experiment*, 2025(8):084004, 2025.
- Nakkiran, P., Neyshabur, B., and Sedghi, H. The deep bootstrap framework: Good online learners are good offline generalizers. *arXiv preprint arXiv:2010.08127*, 2020.
- Njaradi, V., Carrasco-Davis, R., Latham, P. E., and Saxe, A. Optimal learning rate schedule for balancing effort and performance. *arXiv preprint arXiv:2601.07830*, 2026.
- Paquette, E., Paquette, C., Xiao, L., and Pennington, J. 4+3 phases of compute-optimal neural scaling laws. In *The Thirty-eighth Annual Conference on Neural Information Processing Systems*, 2024. URL <https://openreview.net/forum?id=aVSxwicpAk>.
- Pillaud-Vivien, L., Rudi, A., and Bach, F. Statistical optimality of stochastic gradient descent on hard learning problems through multiple passes. *Advances in Neural Information Processing Systems*, 31, 2018.
- Qiu, S., Xiao, L., Wilson, A. G., Pennington, J., and Agarwala, A. Scaling collapse reveals universal dynamics in compute-optimally trained neural networks. *arXiv preprint arXiv:2507.02119*, 2025.
- Rattray, M. and Saad, D. Analysis of on-line training with optimal learning rates. *Physical Review E*, 58(5):6379, 1998.
- Saad, D. and Rattray, M. Globally optimal parameters for on-line learning in multilayer neural networks. *Physical review letters*, 79(13):2578, 1997.
- Smith, S. L., Kindermans, P.-J., Ying, C., and Le, Q. V. Don't decay the learning rate, increase the batch size. *arXiv preprint arXiv:1711.00489*, 2017.
- Varre, A. V., Pillaud-Vivien, L., and Flammarion, N. Last iterate convergence of sgd for least-squares in the interpolation regime. *Advances in Neural Information Processing Systems*, 34:21581–21591, 2021.
- Vyas, N., Morwani, D., Zhao, R., Kwun, M., Shapira, I., Brandfonbrener, D., Janson, L., and Kakade, S. Soap: Improving and stabilizing shampoo using adam. *arXiv preprint arXiv:2409.11321*, 2024.
- Wen, K., Li, Z., Wang, J., Hall, D., Liang, P., and Ma, T. Understanding warmup-stable-decay learning rates: A river valley loss landscape perspective. *arXiv preprint arXiv:2410.05192*, 2024.
- Wu, Y. and Liu, L. Selecting and composing learning rate policies for deep neural networks. *ACM Transactions on Intelligent Systems and Technology*, 14(2):1–25, 2023.
- Yang, G., Hu, E. J., Babuschkin, I., Sidor, S., Liu, X., Farhi, D., Ryder, N., Pachocki, J., Chen, W., and Gao, J. Tensor programs v: Tuning large neural networks

via zero-shot hyperparameter transfer. *arXiv preprint arXiv:2203.03466*, 2022.

Yang, G., Yu, D., Zhu, C., and Hayou, S. Feature learning in infinite-depth neural networks. In *NeurIPS 2023 Workshop on Mathematics of Modern Machine Learning*, 2023.

A. Long-time dynamics

We consider the evolution equation for $c_{t,k}$ in Eq. (4). For small λ_k and recognizing that $\sum_{\ell=1}^N \lambda_\ell c_{t,\ell} = L_t - \sigma^2$, we get

$$c_{t+1,k} \approx (1 - 2\eta_t \lambda_k) c_{t,k} + \frac{\eta_t^2}{m_t} \lambda_k L_t. \quad (18)$$

This recursion admits the solution (Bordelon & Pehlevan, 2022)

$$c_{T,k} = c_{0,k} \prod_{i=0}^{T-1} (1 - 2\eta_i \lambda_k) + \lambda_k \sum_{n=0}^{T-1} \frac{\eta_n^2}{m_n} L_n \prod_{i=n+1}^{T-1} (1 - 2\eta_i \lambda_k). \quad (19)$$

At late times T , and under the power-law assumptions $\lambda_k \sim k^{-b}$ and $(w_k^*)^2 \lambda_k \sim k^{-a}$, we find the relation

$$L_T - \sigma^2 = \sum_k \lambda_k c_{T,k} \approx f_a(2\chi_0) + \int_0^T dt \frac{\eta(t)^2}{m(t)} L_t f_{2b}(2\chi(t)), \quad (20)$$

where $\chi(t) = \int_t^T \eta(t') dt'$, $\chi_0 = \chi(0)$, and

$$f_s(\chi) \equiv \sum_{k=1}^N k^{-s} e^{-k^{-b}\chi}. \quad (21)$$

Note that $df_s(\chi)/d\chi = -f_{s+b}(\chi)$ and that this function has asymptotic behaviors $f_s(\chi) \approx \zeta(s) = \sum_{k \geq 1} k^{-s}$ for small χ (and large N) and $f_s(\chi) \approx \Gamma((s-1)/b)\chi^{(1-s)/b}/b$ for large χ . Approximating $L_t \approx \sigma^2 + f_a(2\chi_0 - 2\chi(t))$, we find

$$L_T - \sigma^2 = \sum_k \lambda_k c_{T,k} \approx f_a(2\chi_0) + \int_0^T dt \frac{\eta(t)^2}{m(t)} [\sigma^2 + f_a(2\chi_0 - 2\chi(t))] f_{2b}(2\chi(t)). \quad (22)$$

B. Analytical derivation of optimal learning-rate schedules

B.1. Power-law spectra

Considering constant batch size $m(t) = m$, from Eq. (22) we get

$$L_T - \sigma^2 \approx f_a(2\chi_0) + \int_0^T dt \mathcal{L}(\dot{\chi}(t), \chi(t)), \quad (23)$$

where $\chi_0 = \chi(0)$,

$$\mathcal{L}(\dot{\chi}(t), \chi(t)) = \dot{\chi}(t)^2 A(\chi, \chi_0), \quad (24)$$

and

$$A(\chi, \chi_0) = \frac{1}{m} [\sigma^2 + f_a(2\chi_0 - 2\chi)] f_{2b}(2\chi). \quad (25)$$

Via Noether's Theorem for time-translation $\frac{d}{dt} \left[\frac{\partial \mathcal{L}}{\partial \dot{\chi}} \dot{\chi} - \mathcal{L} \right] = 0$, we can directly utilize this conservation law

$$\frac{d\mathcal{L}}{d\dot{\chi}} \dot{\chi} - \mathcal{L} = \mathcal{L} = c, \quad (26)$$

for some positive constant c , yielding

$$\dot{\chi}(t) = -\sqrt{\frac{c}{A(\chi(t), \chi_0)}}, \quad (27)$$

where we choose the minus sign as $\chi(t)$ is decreasing with t . By separating variables and imposing $\chi(T) = 0$, we get

$$F(\chi, \chi_0) \equiv \int_0^\chi d\chi' \sqrt{A(\chi', \chi_0)} = \sqrt{c} (T - t). \quad (28)$$

By setting $t = 0$, we find

$$\sqrt{c} = \frac{F(\chi_0, \chi_0)}{T}, \quad (29)$$

yielding

$$\frac{F(\chi, \chi_0)}{F(\chi_0, \chi_0)} = 1 - \frac{t}{T}. \quad (30)$$

For large χ_0 , we find

$$F(\chi_0, \chi_0) \approx \sqrt{\frac{b}{m} \Gamma\left(2 - \frac{1}{b}\right) \sigma^2} (2\chi_0)^{1/(2b)}, \quad (31)$$

and

$$A(\chi_0, \chi_0) \approx \frac{\sigma^2 + \zeta(a)}{m} \frac{\Gamma((2b-1)/b)}{b} (2\chi_0)^{(1-2b)/b}, \quad (32)$$

We now just need to determine χ_0 . We set to zero variations with respect to χ_0 in Eq. (23), yielding (note that \mathcal{L} is also a function of χ_0)

$$-2f_{a+b}(2\chi_0) - \frac{\partial \mathcal{L}}{\partial \dot{\chi}}(t=0) + \int_0^T dt \frac{\partial \mathcal{L}}{\partial \chi_0}(t) = 0. \quad (33)$$

We compute term by term. Using Eq. (27), we find

$$\frac{\partial \mathcal{L}}{\partial \dot{\chi}}(t=0) = 2\dot{\chi}(0)A(\chi_0, \chi_0) = -2\sqrt{c A(\chi_0, \chi_0)}. \quad (34)$$

Additionally,

$$\frac{\partial \mathcal{L}}{\partial \chi_0} = -2\frac{\dot{\chi}^2}{m}f_{a+b}(2\chi_0 - 2\chi)f_{2b}(2\chi) = 2\frac{\dot{\chi}}{m} \frac{F(\chi_0, \chi_0)}{T} \frac{f_{a+b}(2\chi_0 - 2\chi)f_{2b}(2\chi)}{\sqrt{A(\chi, \chi_0)}}. \quad (35)$$

Combining everything together, the condition for χ_0 reads

$$-\frac{\sqrt{mT}}{F(\chi_0, \chi_0)}f_{a+b}(2\chi_0) + 2\sqrt{f_{2b}(2\chi_0)(\sigma^2 + \zeta(a))} - 2 \int_0^{\chi_0} d\chi \frac{\sqrt{f_{2b}(2\chi)}f_{a+b}(2\chi_0 - 2\chi)}{\sqrt{\sigma^2 + f_a(2\chi_0 - 2\chi)}} = 0. \quad (36)$$

We would like to analyze this equation in the large- χ_0 regime. The last term can be approximated as

$$\int_0^{\chi_0} d\chi \frac{\sqrt{f_{2b}(2\chi)}f_{a+b}(2\chi_0 - 2\chi)}{\sqrt{\sigma^2 + f_a(2\chi_0 - 2\chi)}} \approx \int_0^{\infty} dt \frac{\sqrt{f_{2b}(2\chi_0 - 2t)}f_{a+b}(2t)}{\sqrt{\sigma^2 + f_a(2t)}} \approx \sqrt{\frac{1}{b} \Gamma\left(2 - \frac{1}{b}\right)} C (2\chi_0)^{-1+1/(2b)}, \quad (37)$$

where

$$C = \int_0^{\infty} dt \frac{f_{a+b}(2t)}{\sqrt{\sigma^2 + f_a(2t)}} = \sqrt{\sigma^2 + \zeta(a)} - \sigma. \quad (38)$$

Finally, the condition for χ_0 reads

$$-\Gamma((a+b-1)/b)(2\chi_0)^{(1-a-b)/b}/b + \frac{F(\chi_0, \chi_0)}{T} \sqrt{\frac{\sigma^2 \Gamma(2-1/b)(2\chi_0)^{(1-2b)/b}}{m b}} = 0 \quad (39)$$

leading to

$$\chi_0 \approx \frac{1}{2} \left[\frac{m}{b\sigma^2} \frac{\Gamma\left(\frac{a+b-1}{b}\right)}{\Gamma\left(2 - \frac{1}{b}\right)} \right]^{b/a} T^{b/a}. \quad (40)$$

Note that when $b > a$ (hard phase), χ_0 grows superlinearly and hence $\eta(0)$ diverges in T at early times. In this case, the additional constraint $\eta(t) < \eta_{\max}$ must be imposed.

Eq. (27) can be solved explicitly in the scaling limit where t and T are large with t/T fixed. In this limit, both $\chi(t)$ and $\chi_0 - \chi(t)$ are large and hence

$$A(\chi, \chi_0) \approx \frac{\sigma^2}{m} \frac{\Gamma((2b-1)/b)\chi^{(1-2b)/b}}{b} \quad (41)$$

Therefore, Eq. (27) can be rewritten as

$$\dot{\chi}(t) \propto -\chi(t)^{1-1/(2b)}, \quad (42)$$

yielding

$$\int_0^{\chi(t)} d\chi' \chi'^{1/(2b)-1} \propto - \int_T^t dt'. \quad (43)$$

Finally we obtain

$$\chi(t) \approx \chi_0 (1 - t/T)^{2b}. \quad (44)$$

Finally, since $\eta(t) = -\dot{\chi}(t)$, we find

$$\eta(t) \approx \frac{2b\chi_0}{T} (1 - t/T)^{2b-1}, \quad (45)$$

valid in the easy phase $b < a$.

In the hard phase, the constraint $\eta \leq \eta_{\max}$ becomes active and we find the optimal schedule

$$\eta(t) = \begin{cases} \eta_{\max} & \text{for } t < t_s, \\ \eta_{\max} \left(\frac{1-t/T}{1-t_s/T} \right)^{2b-1} & \text{for } t > t_s, \end{cases} \quad (46)$$

where the switching time $0 < t_s < T$ can be determined by minimizing of the generalization error. It is useful to define $\tilde{\eta}(\tau) = \eta(\tau T)$. Then, the loss can be written as

$$L_T - \sigma^2 \sim T^{-(a-1)/b} \left[\int_0^1 d\tau \tilde{\eta}(\tau) \right]^{-(a-1)/b} + \frac{\sigma^2}{m} T^{-(b-1)/b} \int_0^1 d\tau \tilde{\eta}(\tau)^2 \left[\int_{\tau}^1 d\tau' \tilde{\eta}(\tau') \right]^{-\frac{2b-1}{b}}. \quad (47)$$

If $b > a$, the first term will dominate, implying $t_s \approx T$ to leading order. If $b < a$, the second term will dominate. As shown below, the second term is minimized by $t_s = 0$, therefore the constraint $\eta < \eta_{\max}$ is never saturated for $b < a$, in agreement with the easy-phase analysis above. We therefore focus on the case $b > a$ and compute the first-order corrections to $\tau_s \equiv t_s/T \approx 1$.

Using Eq. (46), we find

$$L_T - \sigma^2 \sim T^{-(a-1)/b} f_{\text{Bias}}(\tau_s) + \frac{\sigma^2}{m} T^{-(b-1)/b} f_{\text{Var}}(\tau_s), \quad (48)$$

where

$$f_{\text{Bias}}(\tau_s) = \left[\tau_s + \frac{1 - \tau_s}{2b} \right]^{-(a-1)/b}, \quad (49)$$

and

$$f_{\text{Var}}(\tau_s) = \left[\frac{b}{b-1} \left(\left(\frac{1 - \tau_s}{2b} \right)^{-(b-1)/b} - \left(\tau_s + \frac{1 - \tau_s}{2b} \right)^{-(b-1)/b} \right) + (2b)^{(2b-1)/b} (1 - \tau_s)^{-(b-1)/b} \right] \quad (50)$$

Note that the variance second term is an increasing function of τ_s , confirming that in the easy phase $b < a$, the constraint $\eta(t) < \eta_{\max}$ is never saturated. In the hard case $b > a$, we consider corrections $\tau_s \approx 1 - \epsilon$ and expand to leading order for small ϵ , yielding (up to constants)

$$L_T - \sigma^2 \sim T^{-(a-1)/b} + T^{-(a-1)/b} \epsilon + T^{-(b-1)/b} \epsilon^{-(b-1)/b}. \quad (51)$$

Minimizing this expression over ϵ , we identify the scaling

$$\epsilon \sim T^{-(b-a)/(2b-1)}. \quad (52)$$

Overall, this argument predicts that

$$t_s \approx T(1 - cT^{-(b-a)/(2b-1)}) \quad (53)$$

for some constant c . Figure 7 shows that this prediction agrees with the result obtained by optimizing the full dynamics with CasADI (in that case, for a schedule $\eta(t)$ we define t_s as the first time at which $\eta(t) = 0.95$). As a result, the loss scales as

$$L_T - \sigma^2 \sim T^{-(a-1)/b} + \sigma^2 T^{-(b-1)/b} \epsilon^{-(b-1)/b} \sim T^{-(a-1)/b} + \sigma^2 T^{-(b-1)(a+b-1)/(b(2b-1))}. \quad (54)$$

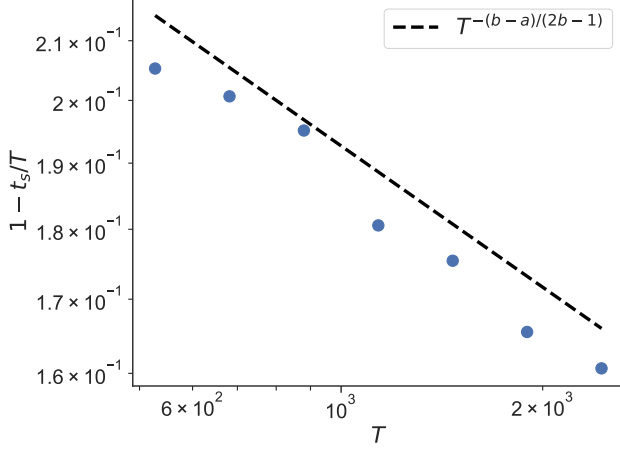


Figure 7. Fraction $1 - t_s/T$ of the total training time spent in the annealing regime. The switching time t_s is defined here as the time at which the schedule $\eta^*(t)$ crosses the level $0.95\eta_{\max}$ for the first time. Same parameters as in Fig. 2a.

C. Comparison with benchmarks

C.1. Constant learning rate

In the case of constant learning rate $\eta_T(t) = \eta_T$, the integral over t in Eq. (22) can be computed, leading to the simplified expression

$$L_T - \sigma^2 \sim (\eta_T T)^{-\frac{a-1}{b}} + \frac{\sigma^2 \eta_T}{m}. \quad (55)$$

Optimizing over η_T , we find $\eta_T \sim T^{-(a-1)/(a+b-1)}$ and $L_T - \sigma^2 \sim T^{-(a-1)/(a+b-1)}$.

C.2. Power-law schedules

In this section, we investigate the optimal power-law schedule $\eta(t) \sim t^{-\delta}$, with $0 < \delta < 1$. We start from the expression

$$L_t - \sigma^2 \sim \left[\int_0^T ds \eta(s) \right]^{-\alpha} + \frac{\sigma^2}{m} \int_0^T dt \eta(t)^2 f_{2b}(\chi(t)) = \text{Bias}(t) + \text{Variance}(t), \quad (56)$$

where $\alpha = (a-1)/b$ and

$$\text{Bias}(t) = \left[\int_0^T ds \eta(s) \right]^{-(a-1)/b} \sim T^{-\alpha(1-\delta)}. \quad (57)$$

The variance integral can be decomposed in two contributions: one from the “bulk” of the integral and one from the region close to the upper limit T .

$$\text{Variance}(t) = \int_0^T dt \eta(t)^2 f_{2b}(\chi(t)) \approx \int_0^{T-\tau} dt \eta(t)^2 f_{2b}(\chi(t)) + \int_{T-\tau}^T dt \eta(t)^2 f_{2b}(\chi(t)). \quad (58)$$

Where we choose τ such that $\chi(T-\tau) \sim \mathcal{O}(1)$, leading

$$\chi(T-\tau) \equiv \int_{T-\tau}^T \eta(t') dt' \sim T^{1-\delta} - (T-\tau)^{1-\delta} \approx \tau T^{-\delta}, \quad (59)$$

so that $\tau \sim T^\delta$. As a consequence, for $t < T-\tau$, we can approximate $f_{2b}(\chi(t)) \approx \chi(t)^{-\gamma} \sim T^{-\gamma(1-\delta)}$ with $\gamma = (2b-1)/b$, while for $t > T-\tau$ $f_{2b}(\chi(t)) \approx \text{constant}$. Therefore,

$$\text{Variance}(t) \sim T^{-\gamma(1-\delta)} \int_0^{T-\tau} dt t^{-2\delta} + \int_{T-\tau}^T dt T^{-2\delta} = T^{-\gamma(1-\delta)} \frac{T^{1-2\delta} - 1}{1 - 2\delta} + T^{-\delta}. \quad (60)$$

Therefore, δ must be chosen to minimize the combination of four terms

$$L_t - \sigma^2 \sim T^{-\alpha(1-\delta)} + T^{-\gamma(1-\delta)} + T^{-\gamma(1-\delta)+1-2\delta} + T^{-\delta}, \quad (61)$$

where we recall that $\alpha = (a-1)/b > 0$ and $1 < \gamma = 2 - 1/b < 2$. We find

$$\delta = \min \left[\frac{\alpha}{\alpha+1}, \frac{\gamma}{\gamma+1} \right] \quad (62)$$

with a crossover between the two regimes at $a = 2b$ and

$$L_T - \sigma^2 \sim T^{-\delta}. \quad (63)$$

Note that for the optimal schedule

$$L_T - \sigma^2 \sim T^{-\min((a-1)/a, (a-1)/b)} \quad (64)$$

so that there is an exponent gap between the optimal and the optimal power law schedules for all $a, b > 1$.

We next consider the scaling of power-law schedules with T -dependent prefactors of the form $\eta(t) \sim T^{-\nu}t^{-\delta}$. Following the same steps as before, we find

$$L_T - \sigma^2 \sim T^{\alpha\nu-\alpha(1-\delta)} + T^{-2\nu-\gamma(1-\delta-\nu)} + T^{-2\nu-\gamma(1-\delta-\nu)+1-2\delta} + T^{-\delta-\nu}. \quad (65)$$

Denoting $x = \delta + \nu$, we can rewrite

$$\mathcal{L}(T) \sim T^{-\alpha(1-x)} + T^{-(\gamma+(2-\gamma)x-2\delta)} + T^{-\gamma+1-(2-\gamma)x} + T^{-x}. \quad (66)$$

Therefore, we can choose $\delta = 0$, leading to a the same scaling behavior as the constant-in- t optimal-in- T schedule.

C.3. General scaling form

In this section, we investigate the performance of scaling form schedules

$$\eta(t) = T^{-\xi}g(t/T), \quad (67)$$

for $\xi \geq 0$. Note that in the easy phase $b < a$, the optimal schedule corresponds to $\xi = 1 - b/a$ and $g(z) \sim (1-z)^{2b-1}$. We find (for $m = 1$)

$$L_T - \sigma^2 \sim \left[\int_0^T dt \eta(t) \right]^{-\alpha} + \sigma^2 \int_0^T dt \eta^2(t) f_{2b} \left(\int_t^T dt' \eta(t') \right), \quad (68)$$

where $\alpha = (a-1)/b$ and $f_{2b}(\chi) = \sum_{k=1}^N k^{-2b} e^{-k^{-b}\chi}$. Plugging the expression in Eq. (67) and changing variables $\tau = t/T$ and $\tau' = t'/T$, we find

$$L_T - \sigma^2 \approx \text{Bias}(T) + \text{Variance}(T), \quad (69)$$

where

$$\text{Bias}(T) = T^{-\alpha(1-\xi)} \left[\int_0^1 d\tau g(\tau) \right]^{-\alpha} \quad (70)$$

and

$$\text{Variance}(T) = \sigma^2 T^{1-2\xi} \int_0^1 d\tau g^2(\tau) f_{2b} \left(T^{1-\xi} \int_\tau^1 d\tau' g(\tau') \right) \quad (71)$$

We recall the asymptotic behaviors $f_s(\chi) \approx \zeta(s) = \sum_{k \geq 1} k^{-s}$ for small χ (and large N) and $f_s(\chi) \approx \Gamma((s-1)/b)\chi^{(1-s)/b}/b$ for large χ . It is then instructive to split the variance integral into an edge component, where $\chi(t) = \int_t^T dt' \eta(t') \ll 1$ and a bulk component where $\chi(t) \gg 1$. To do so, we define t^* so that $\chi(t^*) = 1$, yielding the condition for $\tau^* \equiv t^*/T$

$$\int_{\tau^*}^1 d\tau' g(\tau') = T^{\xi-1}. \quad (72)$$

Assuming $\xi < 1$ (since for $\xi > 1$ the bias increases with T), we get that τ^* is determined by the asymptotic behavior of $g(\tau)$ for $\tau \rightarrow 1$. Assuming $g(\tau) \sim (1 - \tau)^\delta$ with $\delta > 0$, we get

$$(1 - \tau^*) \sim T^{-(1-\xi)/(1+\delta)}. \quad (73)$$

We can then split the variance term into a “bulk” component for $\tau < \tau^*$ and an “edge” component for $\tau > \tau^*$, leading to

$$\text{Variance}(T) \approx \text{Bulk Variance}(T) + \text{Edge Variance}(T). \quad (74)$$

The bulk contribution reads

$$\text{Bulk Variance}(T) \sim T^{1-2\xi} \int_0^{\tau^*} d\tau g^2(\tau) \left(T^{1-\xi} \int_\tau^1 d\tau' g(\tau') \right)^{-\gamma}. \quad (75)$$

For $\delta > (\gamma - 1)/(2 - \gamma) = b - 1$ the integral over τ converges as $\tau^* \rightarrow 1$ and hence

$$\text{Bulk Variance}(T) \sim T^{1-2\xi-\gamma(1-\xi)}. \quad (76)$$

However, if $\delta < b - 1$ there is an additional contribution from the divergence as $\tau^* \rightarrow 1$ for large T , leading to

$$\text{Bulk Variance}(T) \sim T^{-(\delta+\xi)/(\delta+1)}. \quad (77)$$

The edge contribution is

$$\text{Edge Variance}(T) \sim T^{1-2\xi} \int_{\tau^*}^1 d\tau g^2(\tau) \sim T^{1-2\xi} \int_{\tau^*}^1 d\tau (1 - \tau)^{2\delta} \sim T^{1-2\xi} (1 - \tau^*)^{2\delta+1} \quad (78)$$

$$\sim T^{1-2\xi-(1-\xi)(1+2\delta)/(1+\delta)} \sim T^{-(\delta+\xi)/(\delta+1)}. \quad (79)$$

Overall, for $\delta > b - 1$, we get

$$L_T - \sigma^2 \sim T^{-\alpha(1-\xi)} + T^{1-2\xi-\gamma(1-\xi)} + T^{-(\delta+\xi)/(\delta+1)}, \quad (80)$$

while for $\delta < b - 1$ we find

$$L_T - \sigma^2 \sim T^{-\alpha(1-\xi)} + T^{-(\delta+\xi)/(\delta+1)}, \quad (81)$$

Interestingly, for large enough δ , the edge variance terms is negligible and the exponent ξ is obtained by matching the bias and bulk variance terms. In particular, we find $\xi = (a - b)/a$ for $b < a$ (easy phase) and $\xi = 0$ for $b > a$ (hard phase). The corresponding scaling laws are $L_T - \sigma^2 \sim T^{-(a-1)/a}$ for $b < a$ and $L_T - \sigma^2 \sim T^{-(a-1)/b}$ for $b > a$. The scalings match those of the optimal schedule.

C.3.1. THE EDGE TERM IS SUBLEADING FOR THE OPTIMAL SCHEDULE

In the easy phase $b < a$, for the optimal schedule takes the form in Eq. (67) with $\xi = (a - b)/a$ and $\delta = 2b - 1$. This value of δ is chosen to minimize the prefactor of the scaling law. For this value of δ , the edge variance term, which was not included in the derivation of the optimal schedule, is indeed subleading.

We next consider the edge variance term of the optimal schedule in the hard phase $b > a$. Recall that in this phase the optimal learning rate schedule is (taking $\eta_{\max} = 1$)

$$\eta(t) = \begin{cases} 1 & \text{for } t < t_s, \\ \left(\frac{1-t/T}{1-t_s/T}\right)^\delta & \text{for } t > t_s, \end{cases} \quad (82)$$

with $\delta = 2b - 1$ and $T - t_s \sim T^{1-(b-a)/(2b-1)}$. The edge boundary t^* is determined by the condition $\chi(t^*) = 1$, yielding

$$\chi(t^*) = \int_{t^*}^T dt' \eta(t') = \int_{t^*}^T dt' \left(\frac{1-t'/T}{1-t_s/T}\right)^\delta = T\epsilon^{-\delta} (1 - \tau^*)^{\delta+1} = 1, \quad (83)$$

where we have assumed $t_s < t^*$ and we have defined $\epsilon \equiv 1 - t_s/T \sim T^{-(b-a)/(2b-1)}$ and $\tau^* = t^*/T$. Therefore, we get

$$1 - \tau^* = \left(\frac{\epsilon^\delta}{T} \right)^{1/(\delta+1)} \sim T^{-(b-a+1)/(2b)} . \quad (84)$$

Note that $1 - t_s/T > 1 - \tau^*$, confirming that $t_s < t^*$.

The edge variance term reads

$$\text{Edge Variance}(T) = \int_{t^*}^T dt \eta^2(t) = \int_{t^*}^T dt \eta^2(t) = \int_{t^*}^T dt \left(\frac{1 - t/T}{1 - t_s/T} \right)^{2\delta} = (\epsilon T)^{-\delta/(\delta+1)} . \quad (85)$$

The bulk variance term scales as $(\epsilon T)^{-1+1/b}$, confirming that the edge term is subleading.

D. Joint optimization of learning rate and batch size

We want to find the joint optimal schedule of learning rate and batch size that minimizes the final loss. We consider a constraint of the total number of training examples $B_{\text{tot}} = \int_0^T dt m(t)$.

The loss takes the form

$$L_T - \sigma^2 \approx f_a(2\chi_0) + \int_0^T dt \frac{\eta^2(t)}{m(t)} [\sigma^2 + f_a(2\chi_0 - 2\chi(t))] f_{2b}(2\chi(t)) + \mu \int_0^T dt m(t) , \quad (86)$$

where the Lagrange multiplier enforces the constraint on $m(t)$. Optimizing over $m(t)$ yields

$$m(t) = \eta(t) \sqrt{\frac{[\sigma^2 + f_a(2\chi_0 - 2\chi(t))] f_{2b}(2\chi(t))}{\mu}} , \quad (87)$$

with

$$\sqrt{\mu} = \frac{1}{B_{\text{tot}}} \int_0^{\chi_0} d\chi \sqrt{(\sigma^2 + f_a(2\chi_0 - 2\chi)) f_{2b}(2\chi)} . \quad (88)$$

Plugging this expression back into the equation for \mathcal{L}_T , we find

$$L_T - \sigma^2 \approx f_a(2\chi_0) + \frac{1}{B_{\text{tot}}} \left[\int_0^{\chi_0} d\chi \sqrt{(\sigma^2 + f_a(2\chi_0 - 2\chi)) f_{2b}(2\chi)} \right]^2 . \quad (89)$$

Note that this expression is a function of χ_0 only, therefore at fixed χ_0 all learning rate schedules will give the same performance as long as $m(t)$ is chosen appropriately.

For large χ_0 , we find

$$L_T - \sigma^2 \sim \chi_0^{-(a-1)/b} + \chi_0^{1/b}/B_{\text{tot}} , \quad (90)$$

implying that at optimality $\chi_0 \sim B_{\text{tot}}^{b/a}$. This scaling can be achieved in the easy phase ($b < a$), leading to $\mathcal{L}_T \sim B_{\text{tot}}^{-(a-1)/a}$. Note however that χ_0 cannot scale superlinearly with B_{tot} . Indeed, since $\eta(t) \leq \eta_{\text{max}}$ and $m(t) \geq 1$, we have the conditions $\chi_0 \leq \eta_{\text{max}} T$ and $B_{\text{tot}} \geq T$, yielding $\chi_0 \leq \eta_{\text{max}} B_{\text{tot}}$. Therefore, in the hard phase, the optimum is achieved for $\chi_0 \sim B_{\text{tot}} \sim T$, for which $L_T \sim B_{\text{tot}}^{-(a-1)/b}$.

In both easy and hard phases, the degeneracy in the optimization over η and m can be broken by requiring the solution to have the minimum wall-clock time T . This corresponds to taking $\eta(t) = \eta_{\text{max}}$ and

$$m(t) = \frac{B_{\text{tot}}}{2bT} (1 - t/T)^{1/(2b)-1} . \quad (91)$$

In the hard phase, $B_{\text{tot}} \sim T$, so that $m(t)$ remains bounded. However, in the easy phase $T \sim B_{\text{tot}}^{b/a}$ so that the batch size actually grows with B_{tot} as $m(t) \sim B_{\text{tot}}^{1-b/a}$.

E. Loss Dynamics for SGD + Momentum

In this section, we compute the average case loss dynamics over random draws of data. Starting from the following dynamics for $\Delta_t = (\mathbf{w}^* - \mathbf{w}_t)$ and the auxiliary momentum variable $\mathbf{v}(t)$, we track the following updates

$$\Delta_{t+1} = \Delta_t - \eta_t \mathbf{v}_t, \quad \mathbf{v}_t = (1 - \beta_t) \mathbf{v}_{t-1} + \beta_t \mathbf{g}_t, \quad \mathbf{g}_t = \frac{1}{m} \sum_{\mu=1}^m \tilde{\psi}_{\mu,t} [\tilde{\psi}_{\mu,t} \cdot \Delta_t + \sigma \epsilon_{\mu,t}] \quad (92)$$

To compute the test loss, we need to track the following three correlation functions

$$C_{k,t} = \langle \Delta_{k,t}^2 \rangle, \quad V_{k,t} = \langle v_{k,t}^2 \rangle, \quad R_{k,t} = \langle \Delta_{k,t} v_{k,t} \rangle \quad (93)$$

where the average is computed over the random samples from each minibatch. These three variables evolve according to the following linear dynamics

$$\begin{aligned} C_{k,t+1} &= C_{k,t} - 2\eta_t R_{k,t} + \eta_t^2 V_{k,t} \\ V_{k,t+1} &= (1 - \beta_t)^2 V_{k,t} + 2\beta_t (1 - \beta_t) \lambda_k (R_{k,t} - \eta_t V_{k,t}) + \beta_t^2 \left[\frac{m+1}{m} \lambda_k^2 C_{k,t+1} + \frac{1}{m} \lambda_k \sum_{\ell} \lambda_{\ell} C_{\ell,t+1} + \frac{\sigma^2}{m} \lambda_k \right] \\ R_{k,t+1} &= (1 - \beta_t) (R_{k,t} - \eta_t V_{k,t}) + \beta_t \lambda_k C_{k,t+1} \end{aligned} \quad (94)$$

We note that due to the time indexing that we adopted above, the right hand side for the equations defining the dynamics for $R_{k,t+1}$ and $V_{k,t+1}$ depend on $C_{k,t+1}$ rather than $C_{k,t}$ (though of course this can be substituted).² The loss function dynamics, as before, can be computed from $C_{k,t}$,

$$L_t - \sigma^2 = \sum_k \lambda_k C_{k,t}. \quad (95)$$

We use the above dynamics for $\{C_{k,t}, R_{k,t}, V_{k,t}\}$.

F. Optimal Control Implementation

To determine the optimal learning rate schedules numerically, we formulate the problem as a discrete-time optimal control problem governed by the recursive evolution of $c_{t,k}$ (Eq. (4)). We employ a direct single-shooting method to transcribe this control problem into a non-linear programming (NLP) problem. In this formulation, the control inputs (the learning rate η_t and optionally the batch size m_t) are treated as the primary decision variables. The state trajectory is not included in the set of decision variables. The objective function, defined as the terminal generalization error L_T , is thus expressed as a direct function of the initial conditions and the sequence of control inputs.

We implement this optimization framework using CasADi (Andersson et al., 2019), which performs automatic differentiation to efficiently compute the necessary gradients of the objective with respect to the control trajectory. The resulting NLP is solved using IPOPT (Interior Point OPTimizer), a primal-dual interior-point method. To ensure computational efficiency for large horizons, we configure the solver to use a limited-memory approximation of the Hessian and the MUMPS linear solver for the internal step computations. The implementation of our optimization framework is available in the supplementary material.

²We find this convention yields better stability than defining the dynamics as $\Delta_{t+1} = \Delta_t - \eta_t \mathbf{v}_t$ where $\mathbf{v}_t = (1 - \beta_t) \mathbf{v}_{t-1} + \beta_t \mathbf{g}_{t-1}$.